Engineering Structures 317 (2024) 118652

Contents lists available at ScienceDirect

Engineering Structures

journal homepage: www.elsevier.com/locate/engstruct

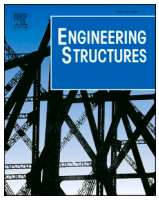

Efficiency of FRPU strengthening of a damaged masonry infill wall under in-plane cyclic shear loading and elevated temperatures

Petra Triller [a], Konrad Kwiecień [b], Arkadiusz Kwiecień [c,*], Uroš Bohinc [a], Bogusław Zając [c], Marcin Tekieli [c], Magdalena Szumera [b], Theodoros Rousakis [d], Vachan Vanian [d], Ahmet Tugrul Akyildiz [c], Alberto Viskovic [e]

[a] Slovenian National Building and Civil Engineering Institute (ZAG), 1000 Ljubljana, Slovenia
[b] AGH University of Science and Technology, Faculty of Materials Science and Ceramics, 30-059 Cracow, Poland
[c] Cracow University of Technology, Faculty of Civil Engineering, 31-155 Cracow, Poland
[d] Democritus University of Thrace, Department of Civil Engineering, GR-67 100 Xanthi, Greece
[e] University "G. d'Annunzio" of Chieti, 65127 Chieti, Pescara, Italy

ARTICLE INFO

Keywords:
Masonry blocks
Damaged infill
FRPU
External composite strengthening
In-plane shear
Thermal tests
DIC measurements

ABSTRACT

This paper presents results of in-plane shear tests carried out at the ZAG laboratory in Ljubljana (Slovenia) on a RC frame with masonry infill made of clay blocks (KEBE OrthoBlock). The frame was loaded with constant vertical loads at the top of the columns and then by gradually increasing horizontal cyclic loads at the top beam level. Acquired forces and measured displacements allowed capturing hysteretic behavior for determination of dissipation energy. In addition, two Digital Image Correlation (DIC) systems, Aramis and the CivEng Vision, were used to visualize the behavior of the tested specimens, with an emphasis on computing locally required information about the behavior of highly deformable interfaces. Three types of specimens were tested in-plane: the reference specimen in form of plain RC frame, the reference specimen with constructed masonry infill without any strengthening and the specimen, previously damaged and then strengthened on both sides using glass mesh bonded to the infill and the RC frame using flexible adhesive made of polyurethane matrix (Glass Fiber Reinforced PolyUrethane - GFRPU system). The strengthening process, allowed the specimen to withstand additional cyclic loads, reaching a maximum drift of 3.6 % without serious damage disqualifying the structure from further exploitation. The GFRPU strengthening system was found to be highly effective in preventing infill collapse of damaged masonry infill wall during in-plane loading. Additionally, the results of extended thermal analysis of PU are presented as polymers are, in general, a material, poorly resistant to heat. However, the analyzed PU manifested stable properties up to 200 degrees Celsius, which makes this material promising in civil engineering applications at elevated temperatures.

1. Introduction

Earthquake loads play a significant role in terms of external forces acting on buildings in seismic areas. In such structures, high displacement and ductility demands emerge on the masonry members, particularly the infill walls in RC framed constructions [1–3]. Infill walls increase the rigidity of structural systems, making buildings more resistant to horizontal forces than bare-framed structures [4,5]. However, the contribution and possible effects of infills are often neglected during the design phase. The brittle characteristics of traditional infill materials can lead to sudden brittle damage under loads exceeding their elastic capacities, causing a lack of ductility in the structural system.

Masonry infill walls may experience substantial damage due to excessive deformation [6,7]. The most common failures are mainly due to interaction effects at the wall-frame interfaces, leading to connection loss and eventual partial or total collapse. Such damages are a main cause of casualties during earthquakes, with destructive effects like out-of-plane failures and deterioration of structural and dynamic characteristics [8]. In [9], a three-story full-scale RC building was tested with and without infill walls. The study reported that the drift capacity with infills was 1.5 % and highlighted that up to this drift level, the infills helped control inter-story drifts as long as out-of-plane failure was

* Corresponding author.
E-mail address: akwiecie@pk.edu.pl (A. Kwiecień).

https://doi.org/10.1016/j.engstruct.2024.118652
Received 22 January 2024; Received in revised form 23 June 2024; Accepted 17 July 2024
Available online 29 July 2024

prevented. In another study [10], a five-story full-scale hybrid (experimental and numerical) simulated building was subjected to pseudo dynamic tests. The study identified four Limit States correlated to drift (DL) ratios. DL1 (0.09 %): first interface cracks, DL2 (0.39 %): corner crushing and sliding, DL3 (0.75 %): wide cracks and brick crushing, DL4: near collapse (not reached). Their findings also indicate the need for out-of-plane collapse prevention mechanisms in infills subjected to higher drift ratios.

The connection between the infill and RC frame has substantial importance when ductility in the structural system is considered. Some research is already focusing on this challenge [11–14]. It is especially important during the assessment of seismic damages [15,16] and the evaluation of the cost of repair [17]. Many various strengthening techniques for infill walls have been studied and examined experimentally [18–20]. One of the tested solutions is the external strengthening of infill walls with various composite materials [21,22]. Such solution was tested mainly during in-plane cyclic shear tests [23]. In those cyclic tests, the problem of connection loss at the RC frame and infill interfaces was reported [24]. To improve this drawback, flexible polyurethane (PU) can be used to bond various composite fibers to the weak masonry substrate to form Fiber Reinforced PolyUrethane (FRPU) as well as to repair damaged RC frames. The economic efficiency of this FRPU system in a real infilled RC frame building located in a seismic area was analyzed by [25]. Moreover, FRPU may be used to create flexible connections between frames and infills to form innovative protection along the frame-infill interface.

FRPU is suitable for emergency applications, as it cures within hours and is easily applicable. The initial application of glass FRPU in emergency scenarios was documented by [26] in the protection of masonry walls against cyclic loads. The efficiency of this FRPU system was compared to Glass Fibre Reinforced Polymer (GFRP) and Fibre Reinforced Cementitious Mortar (FRCM) strengthening [27]. The study reported that FRPU cured very fast (few hours) and did not lose bond with masonry even at extreme deformations.

The same glass FRPU system was applied as emergency strengthening of masonry infill detached from an RC frame and tested under quasi-static in-plane cyclic shear load up to 3.6 % of the frame horizontal drift. Results of this in-plane test are compared in this paper with results of in-plane tests obtained for a plain RC frame and an RC frame with infill. The use of two Digital Image Correlation (DIC) methods, Aramis [28] and CivEng Vision [29] allowed visualizing characteristic deformations of RC frames and the infill as well as presenting strain fields observed at interfaces between them, where the failure occurred mainly.

Although the protective impact of FRPU systems on masonry infill walls was proven, the use of polymers as adhesive connecting building elements may raise a safety concern not only in relation to in-plane and out-of-plane movements. One of the possible durability issues is the thermal degradation of the material, as polymers are, in general, much less resistant to heat than mineral building materials. FRCM composites have proven to be very effective for both in-plane and out-of-plane loading of infilled frames [30–33], overcoming some issues with traditional FRP systems. Some of these are but not limited to: a) Poor long-term temperature resistance - FRP loses strength and effectiveness at elevated temperatures, especially above the glass transition temperature of the epoxy resin/adhesive; b) Aging and degradation from UV exposure - FRP is susceptible to aging and degradation of mechanical properties when exposed to UV light, wind, rain, snow, etc.; c) Low fire resistance - the epoxy resins used in FRP have poor fire resistance compared to the non-combustible mortar matrix of TRM. The superior performance of FRCM as a strengthening material at high temperatures compared to traditional FRPs has been demonstrated in the following studies [34–36]. Especially for shear and flexural strengthening comparison of TRM vs FRPs was conducted in previous studies when subjected to high-temperature. Study from [37] indicate TRM exhibits excellent behavior in flexural strengthening of RC beams at elevated temperatures, maintaining an average effective-ness of 55 % compared to its effectiveness at ambient temperature, whereas FRP systems lose their effectiveness entirely. Similarly, TRM has been shown to outperform FRP in shear strengthening of RC beams at high temperatures, with TRM jackets improving the shear capacity of RC beams exposed to varying high temperatures [38]. Furthermore, bond performance between TRM and concrete interfaces has been shown to be superior to that of FRP at high temperatures, with TRM specimens maintaining an average of 85 % of their ambient bond strength up to 400 °C, while FRP specimens maintained only 17 % at 150 °C [39]. For epoxy resins, which are the most common group of polymers used in civil engineering, high temperatures pose a significant danger. For typical epoxy resin, its glass transition temperature is in the temperature range of 60 °C. Polyurethanes are usually superior to epoxy resins in this field, as they start degrading above 200 °C with urethane link disintegration [40]. The preliminary studies were indeed able to confirm no thermal degradation below 200 °C of the polymer used as the matrix for mentioned composite systems [41]. However, it was not evaluated how the performance of the polymer matrix would change at higher temperatures, e.g. in case of earthquake-induced fire.

Moreover, the FRPU strengthening overcame the drawbacks of composite FRP and FRCM strengthening systems related to stress concentrations causing damages at low levels of drifts. However, FRCM systems are reported to be resistant to elevated temperatures (even fire) [34,35], but FRP ones lose their properties in relatively low ranges of elevated temperatures due to the low glass transition temperature of epoxy adhesives (around 60 °C). Because of elevated temperatures occurring in hot countries or at the beginning of fire (often present during earthquakes), checking of thermal stability of the polyurethane flexible adhesive is required, when such protection is considered in seismic areas. Thus, a thermal stability investigation of the polyurethane-based FRPU was carried out in this research.

The objective of this work is to present the ability of the newly proposed flexible FRPU strengthening to preserve the in-plane seismic performance of damaged masonry infills in RC frame structures and prevent out-of-plane collapse of infills. The proposed FRPU solution, based on a special polyurethane adhesive, was examined in an initial cyclic shear test, manifesting high resistance even after large in-plane drifts over 3.5 %. The aim was to assess the value of applying this innovative FRPU solution in an expensive natural scale shake table test. Moreover, a thermal stability investigation of the polyurethane based FRPU was carried out, as checking thermal stability is required when considering such protection in seismic areas prone to elevated temperatures. The presented thermal research indicates the applied PU has noteworthy stability, differing from polymeric materials commonly used in civil engineering.

2. Experimental program and strengthening procedure

2.1. Experimental setup

The in-plane experiments were carried out at the Slovenian National Building and Civil Engineering Institute (ZAG) in Ljubljana. Two identical RC frames were constructed, one plain A1F (Fig. 1), and one with an infill wall (A2) made of hollow clay blocks (KEBE OrthoBlock), see Fig. 1. All specimens were constructed at a scale of 1:1.

The tested RC frames consisted of a beam, column, and foundation elements. Both beam and column members had section dimensions of 25 cm × 25 cm. The foundation was designed to be stronger than the upper frame and its dimensions in height and width were 40 cm and 30 cm, respectively. Reinforcement details and a view of the infill wall are shown in Fig. 1.

Three different types of mortar were used in the experiment. For the infill, thin layer mortar (M10) was used as bonding material on the brick interfaces. Cementitious mortar was applied for the connection between the infill and the RC frame (A2). In addition, injection grout was used to fill some undesirable existing gaps at the interfaces, which were left after

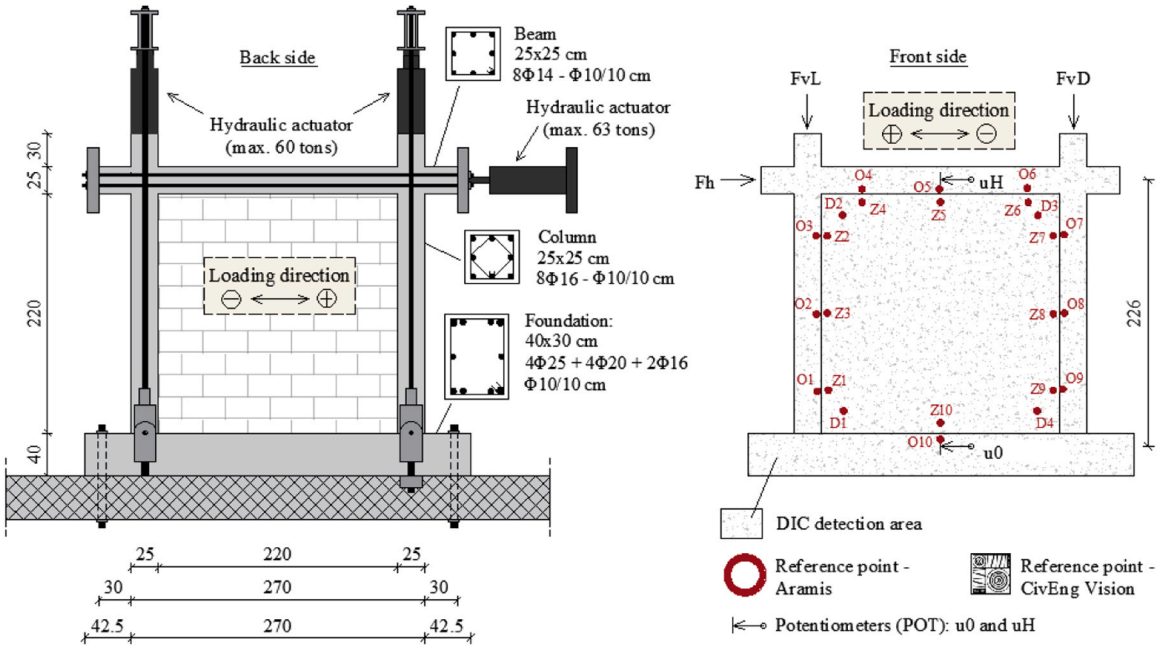

Fig. 1. Back and front view of the RC frame with infill wall: dimensions in [cm], reinforcement details, test setup, DIC detection area and DIC reference points – the CivEng Vision were located at the whole surface every 20–30 cm (see Figs. 13b and 15b).

the handmade mortar application. The grout was applied to the interface using hand pistols with low-pressure injection. It ensures as good workmanship for cyclic tests of infills as possible and thus perfect mineral adhesiveness.

The strength of the thin layer as well as cementitious mortar and injection grout was determined on prisms (40/40/160 mm) at the time of testing the walls (average age of 188, 190, and 46 days, respectively). The average value of compressive strength of thin layer mortar, measured on 60 specimens, was 10.2 MPa (± 21.2 %), and the average flexural strength, measured on 30 specimens, was 4.5 MPa (± 16.9 %). The average compressive strength of cementitious mortar, measured on 36 specimens, was 30.4 MPa (± 24.7 %) and the average flexural strength, measured on 18 specimens, was 7.2 MPa (± 16.7 %). The average compressive strength of injection grout, measured on 16 prisms, amounted to 53.1 MPa (± 13.1 %), and its average flexural strength was 4.7 MPa (± 18.8 %). The average compressive strength of concrete was determined on three 150/150/150 mm cubes and reached 46.9 MPa (± 6.0 %). All values presented above are average values determined in accordance with EN 1015–11 and EN 12390–3. Steel reinforcement RA B500B was used for concrete elements of the wall specimens. The yield and ultimate tensile strength of steel were determined by uniaxial tensile testing according to EN ISO 6892–1:2016. The obtained values of yield and ultimate tensile strengths were 534.0 MPa and 644.0 MPa, respectively.

The testing program is presented in Table 1. The specimen A1F was tested in-plane under cyclic shear. The specimen A2 was also tested in-plane both in its original state (specimen A2) as well as in the strengthened state (A2R). The test setup and test instrumentation for both types of experiments are presented in Fig. 1.

Table 1
Experimental programme.

Specimen	Strengthening state	Infills
A1F	Unstrengthened	No
A2	Unstrengthened	Yes
A2R	Strengthened	Yes

2.2. Instrumentation

To acquire results of the in-plane tests, displacement transducers (potentiometers - POT) were placed on the back side of specimens, see Fig. 1. In addition, optical measurement systems based on Digital Image Correlation (DIC) technique were used on the front side of frames, as schematically shown in Fig. 1, which enabled the visualization of the specimens' behavior. Multiple reference points were identified both on the frames and infill walls for each specimen, covering the entire frame-wall perimeter. Fig. 1 shows the setup and reference points for the A2R frame. The DIC technique was used to measure and visualize the deformation of the FRPU bonded to the infill and RC frame. The displacement field over the entire surface of the specimen was measured with two DIC systems: 3D GOM ARAMIS 5 M and 2D DIC system CivEng Vision, developed at the Cracow University of Technology. In the GOM ARAMIS 5 M vision system, 2 cameras with a resolution of 5 Mpx were used, while the CivEng Vision system employed a single lens reflex camera (DSLR) with a resolution of 20.9 Mpx. The photos were taken using the manual settings of the aperture, shutter speed, and ISO value, without image compression. RAW files were processed using optical measurement systems. The acquisition rate of the DIC system GOM ARAMIS 5 M was 1 image per 5 s

To ensure optimal performance of the optical system, monitored surfaces were painted with a quasi-random pattern - for ARAMIS, and points considered for analysis are presented in Fig. 1. Proper resolution of DIC measurements using CivEng Vision was assured by special artificial markers glued on the painted surface (see Fig. 1), whereas measurement accuracy for CivEng Vision was presented in detail by [29].

2.3. Testing Procedure

During the in-plane tests, the frames were loaded with 375 kN vertical load on each column, which results in a normalized axial force of 0.3. The latter simulates the behavior of the lower floor frame in a multi-story building. The horizontal load was imposed quasi-statically in cycles. The loading cycles consisted of identical steps for all frames. Details of the typical loading scheme are shown in Fig. 2 in the form of a drift ratio calculated from POT ((uH-u0)/226 cm). For each drift ratio (loading phase), three horizontal loading cycles were performed with a

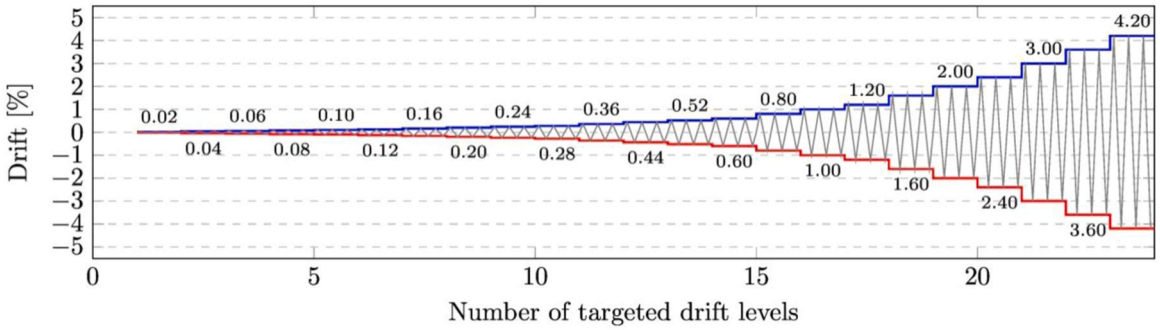

Fig. 2. Loading cycles of the horizontal excitation.

constant displacement rate of the horizontal actuator. The displacement rate was adjusted so that each loading phase lasted approximately 20 min to complete.

The displacement field of the DIC Aramis measurements is presented for the infills, as part of the painted surface of the RC frame was covered by tie-rods and was not visible in the camera, which prevented the computation of all reference points at all times. Discrete markers were processed separately: for GOM ARAMIS systems 3D positions of markers were produced whereas the CivEng Vision markers produced 2D positions. Since the markers were placed on both the RC frame and the infill, a quantitative study of the interface behavior was possible.

2.4. Strengthening Procedure

The in-plane tests were performed on unstrengthened specimen A2 as well as on specimen A2R, which represented the damaged A2 specimen, strengthened using the FRPU (Fiber Reinforced PolyUrethane) system. Before the strengthening of the specimen A2, complete detachment of the infill from the frame and corners crushing were noticed. There was no remaining permanent deformation of the RC frame due to its elastic behavior. The damaged infill was strengthened and not removed. The strengthening process began by covering the damaged and not repaired infills with PU ZP Primer. Following this, glass fibers bands made of Wrap 350 G Grid were cut and temporarily fastened to the infill surface. The composite was then constructed by bonding the bands with PU PS. The gaps from collapsed masonry in specimen A2 were covered by the FRPU system in specimen A2R without the application of mortars, as the FRPU system was applied as an emergency method on both sides over the entire surface of the A2 infill. Glass fibers of the FRPU composite were connected by the polyurethane adhesive to the infill, curved at the infill-frame contact and then attached to all edges of the frame (bonding width – 5 cm). The elastic modulus, strength, and ultimate elongation of the polymer, provided by the manufacturer, were 16 MPa, 2.5 MPa, and 40 %, respectively. The GFRP mesh weighs 360 g/m^2. In the tensile test, the elastic modulus, strength, and ultimate elongation of the GFRP mesh were 80 GPa, 2.6 GPa, and 4 %, respectively. The strengthening process is presented in Fig. 3. The A2 specimen, strengthened using the abovementioned strengthening technique, is hereinafter referred to as A2R. After the strengthening procedure of the A2R specimen was finished, the entire surface of one side of the infill has been painted white and dotted using a speckle pattern in order to ensure optimal performance of the Aramis DIC and the CivEng Vision DIC system (Fig. 1).

2.5. Thermal analysis

The solar heating capacity was evaluated by exposing the FRPU to solar radiation. The measurements were performed with an infrared thermometer in Cracow, Poland (latitude 50°N) on 06/28/2021 between 12–5 p.m. each 0.5 h (solar elevation 63°−24.5°). The atmospheric temperature was 27 °C. The matrices used in the experiment were made of polyurethanes of type PS, PST, and PT, and of an epoxy resin – S330.

The PS polyurethane was chosen for thermal analysis – the same was used as the matrix for the FRPU strengthening of the specimen A2R. The thermal analyses were carried out on either grated (DSC-TGA) or excised (dilatometry, HSM) specimens. The DSC-TGA analysis was conducted in STA 449 F3 Jupiter 7 (NETZSCH-Gerätebau GmbH, 95100 Selb, Germany) operating in the heat flux DSC mode in the atmosphere of synthetic air (40 mL/min). The applied temperature range was between ambient to 600 °C at a heating rate of 10 °C/min. The sample was in the form of granules (6 mg) and was placed in an aluminum crucible. Dilatometric measurements were conducted in DIL 402 C dilatometer (NETZSCH-Gerätebau GmbH, 95100 Selb, Germany) in the atmosphere

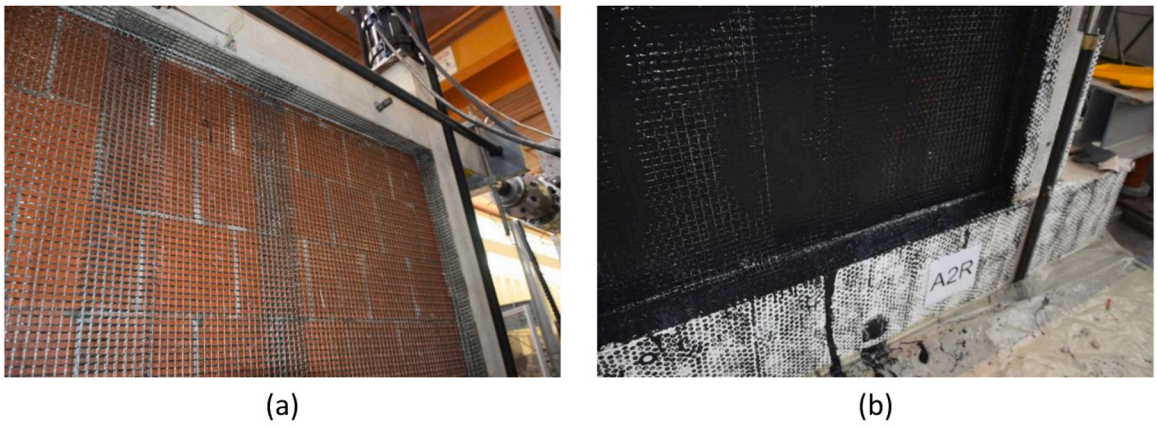

Fig. 3. Strengthening procedure for specimen A2R: (a) first stage – attachment of GFRP reinforcement mesh on the infill; (b) second stage - gluing of the mesh on the infill using flexible polyurethane matrix.

of synthetic air. The applied temperature was between ambient and 240 °C with a heating rate of 5 °C/min and the force range (load at the sample) was 0.01 N. The sample excised to a length of 10 mm was placed in a holder system made out of Al2O3.

The morphological changes of the analyzed material during heating were observed using a hot-stage microscope (HSM) Misura Expert System Solutions coupled with software Misura 3.32 HSM. The samples were prepared in 3 × 3 x 2 mm cuboid form and measured with a heating rate of 10 °C/min up to the melting temperature.

3. Results and discussion

3.1. In-plane tests

Maximum displacements in loading cycles and maximum drifts in loading cycles are presented in Fig. 2. The same testing protocol was applied for all tested specimens.

The bare frame specimen of the experimental campaign, named A1F, was tested as a reference up to a drift of 4.3 %. The behavior of the specimen was linear elastic up to a drift of approximately 0.35 %. In the following cycles, slight stiffness degradation started to be observed in the force-displacement curve, but no noticeable cracks or damage were observed in the front view of the specimen. This observation can also be verified from the force-displacement curve, where the width of the hysteretic curve did not alter significantly during the sequential loading. The first noticeable crack was observed approximately at the drift ratio of 3.00 % at the left bottom column of the specimen. After this drift, the cracks propagated in the critical region of the column base, and afterwards, at approximately 4.30 % drift, significant crushing of the concrete at the critical regions adjacent to the beam-column joints occurred (Fig. 4a).

In the case of A2, partial detachment at the frame-infill interface was clearly observed at 0.44 % drift, while the DIC results of major strain showed that the first damage occurred even earlier, at 0.20 % drift. Based on the DIC measurements the lifting of the infill in the lower corners at the contact with the RC foundation started already in the 3rd loading phase, in which the drift amounted to 0.06 %. As the load increased, the deformations at the bottom horizontal RC foundation-infill interface increased. At the same time, in accordance with the direction of loading, the bed-joint at the corner between the penultimate and last row of the infill began to open (see Figs. 5a and 6a). In the subsequent stages, there was a loss of the top horizontal RC beam-infill interface. In the penultimate loading phase of the test, in which the 1.20 % drift was imposed, the outer wall of the multihole brick (orthoblock) at the right bottom corner started to crush.

Complete detachment and crushing at the corners was obtained at 1.60 % drift (see Fig. 5b), and next the test of the A2 specimen was stopped (Fig. 5b). The infill wall was susceptible to out-of-plane collapse and required strengthening. The corresponding base shear force of the A2 frame at this drift level (considering the average of the positive and negative loading direction) was 178 kN. Sliding of the top and bottom RC beam-infill interface was the main mechanism which developed due to the applied shear load.

The efficiency of the FRPU strengthening system (A2R specimen) was tested by the same quasi-static cyclic test (Fig. 2) as used for the unstrengthened specimen A2. The behavior of the specimen, observed during the test and based on the DIC measurements, is described below. Major strain distribution shows that first damage was rocking, observed as opening and closing of the vertical and horizontal RC frame-infill interface, which occurred at drift of 0.08 %. In the next loading stages, the gap between the infill and the RC frame became wider, while still no detachment of the GFRP reinforcement mesh was observed. According to the increasing imposed displacements, the damage spread to corner areas (see bulge in the infill behind the working FRPU strengthening in the bottom left and top right corners in Fig. 5c).

At drift of 0.80 %, the first visible damage during the test - crushing of bricks in the upper horizontal RC beam-infill interface - occurred. At drift of 1.00 %, there was a visible deflection of the mesh and the infill deviated from the RC frame in the interface, besides some cracks in the upper RC beam appeared. At 1.20 % drift, there was a local detachment of the mesh from the masonry infill in the bottom back corner as well as in the upper back corner of the specimen. Some cracks in the columns appeared. At 1.60 % drift, first diagonal cracks of the masonry infill appeared in the centre of the specimen but without rupture of the mesh. There was observed local detachment of the mesh at the edges and the mesh was torn locally at the bottom edge. When the drift of 2.00 % was imposed, there were observed more local delaminations between the infill and the mesh, in places where crushed sharp masonry particles moved out-of-plane. In the following steps, the existing cracks widened and some new appeared in the infill and in the RC columns. The maximum level of drift ratio was defined by maximum displacement of the horizontal hydraulic actuator (100 mm). Major damage occurred at the infill-RC frame interface in both the infill and in the mesh (see Figs. 5d and 6b). It was mainly crushing of masonry blocks between the FRPU mesh layers and single local detachments of the mesh from the concrete surface.

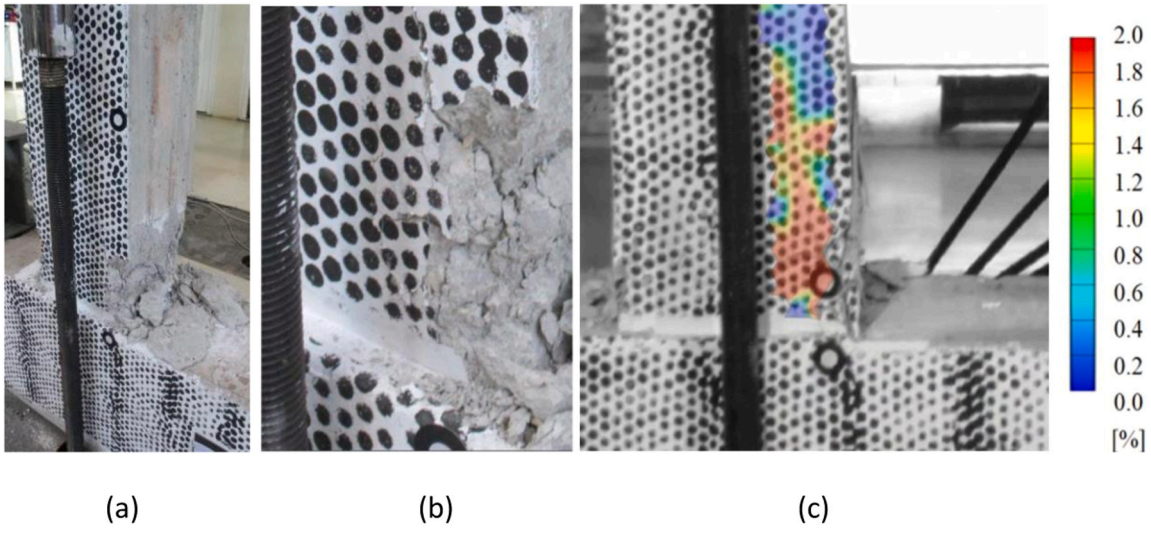

Fig. 4. Concrete crushing of the A1F specimen at 4.3 % of the frame horizontal drift: (a) damage at foundation-column joint; (b) large deformation in the main crack surrounding; (c) major strain results of the optical DIC system (2.0 % of strain) in the location of (b), at the end of the test.

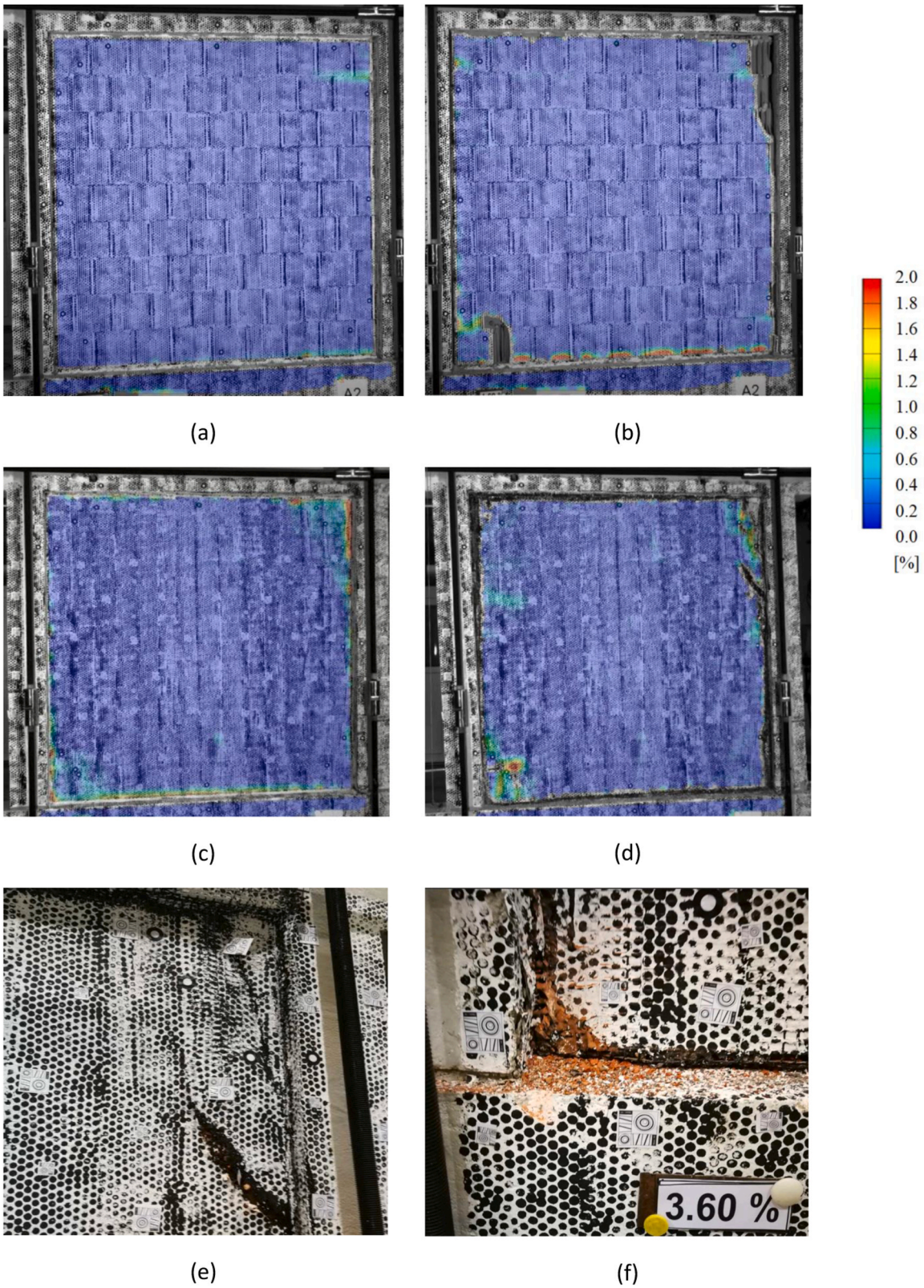

Fig. 5. Major strain distribution of the optical Aramis DIC system: (a) A2 specimen at 0.24 % drift, (b) A2 specimen at 1.60 % drift, (c) A2R specimen at 0.20 % drift, (d) A2R specimen at 3.60 % drift, (e) crushed top right corner at 3.60 % drift, (f) crushed bottom left corner at 3.60 % drift.

Generally, FRPU connecting properties were not lost. Based on the damage observed in the RC frame (see Fig. 6c), it is assumed that the stresses in the steel reinforcement exceeded the yield strength. The condition of the strengthened specimen at this stage is presented in Fig. 6d.

Based on the observed behavior, it can be concluded that local damage of the strengthened specimen occurred. Especially, the sliding of the top and bottom RC beam-infill interface took a significant share as

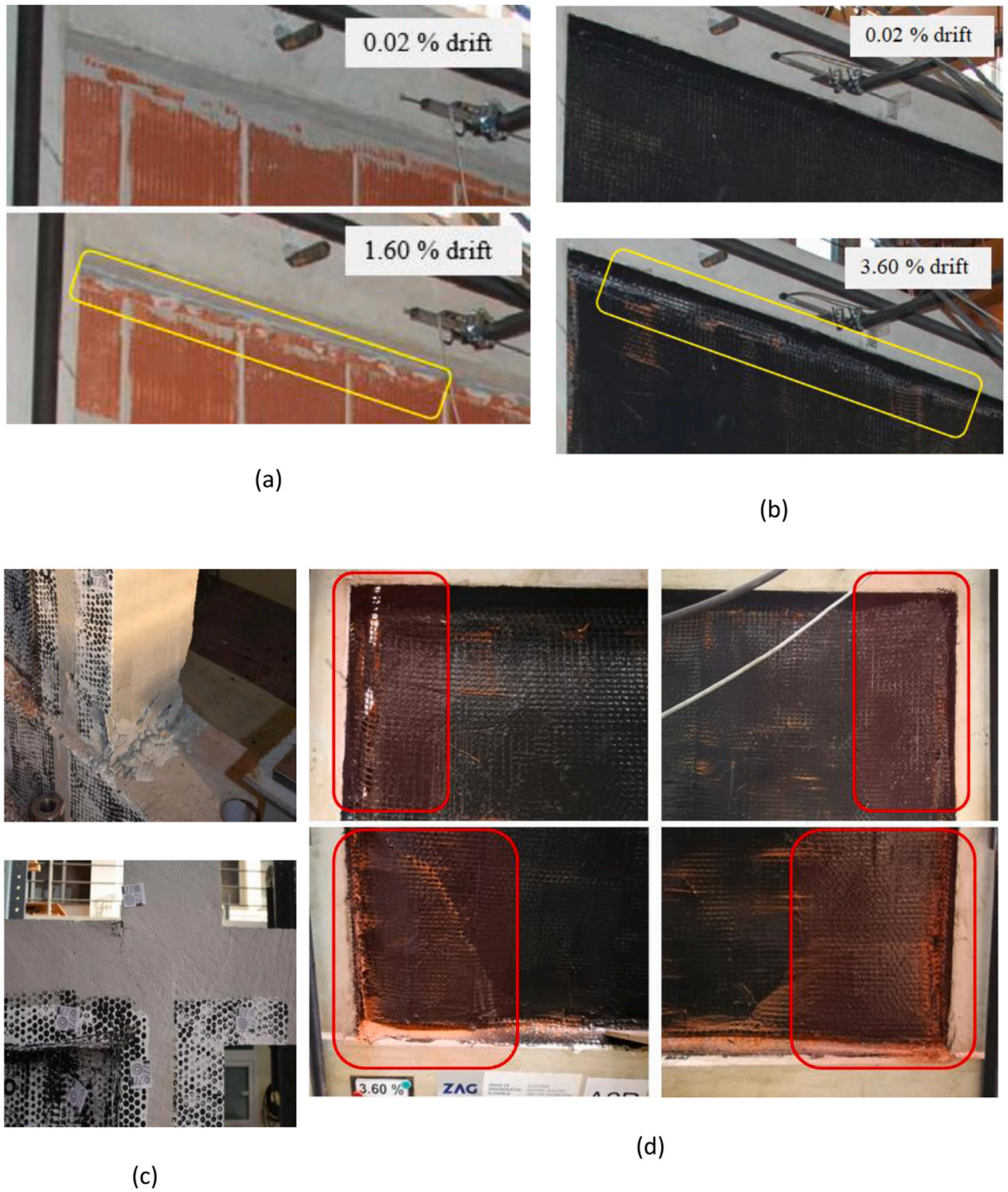

Fig. 6. Damage and deformation at top infill interface: (a) A2 specimen at 0.02 % and 1.6 % drift (front view), (b) A2R specimen at 0.02 % and 3.6 % drift (front view), (c) Front view of A2R specimen at 3.6 % drift: Cracks at bottom and top of columns, (d) Back side view of A2R specimen before 3.6 % drift: Damage and detachment of infill at interfaces but FRPU strengthening is still functional.

well as crushing effect at masonry side interface caused by the applied shear load. On the other hand, no crucial global detachment occurred between FRPU strengthening and supporting structural surfaces (masonry and concrete) until the end of the test (see Fig. 7b), even when the shear displacement applied on the strengthened specimen A2R was much larger than on the unstrengthened one A2 (see Fig. 7). The x-axis in Figs. 7, 9 and 10 represents the total distance traveled defined as:

$$d_{total} = \sum |uH(t) - u0(t)| \quad (1)$$

Total distance is employed here since it enables time independent visualization and facilitates focus on the damage evolution.

Comparison of the load-drift hysteretic curves obtained for the levels of maximum drifts (end of the individual test) for each of the tested specimens A1F, A2 and A2R is presented in Fig. 8. The 1.6 % drift level provides a consistent point of comparison across all three specimens. The corresponding base shear force of the A1F, A2 and A2R frames at drift level of 1.6 % (considering the average of the positive and negative loading direction) was 128 kN, 178 kN and 179 kN, respectively. By comparing the base shear force at this drift level, it is possible to accurately assess the impact of the infill and the strengthening technique on the frame's capacity. The presence of the infill increases the RC frame capacity by about 39 %. It should be noted that despite the loss of the bond between the brick-infill and RC frame as well as the minor damages

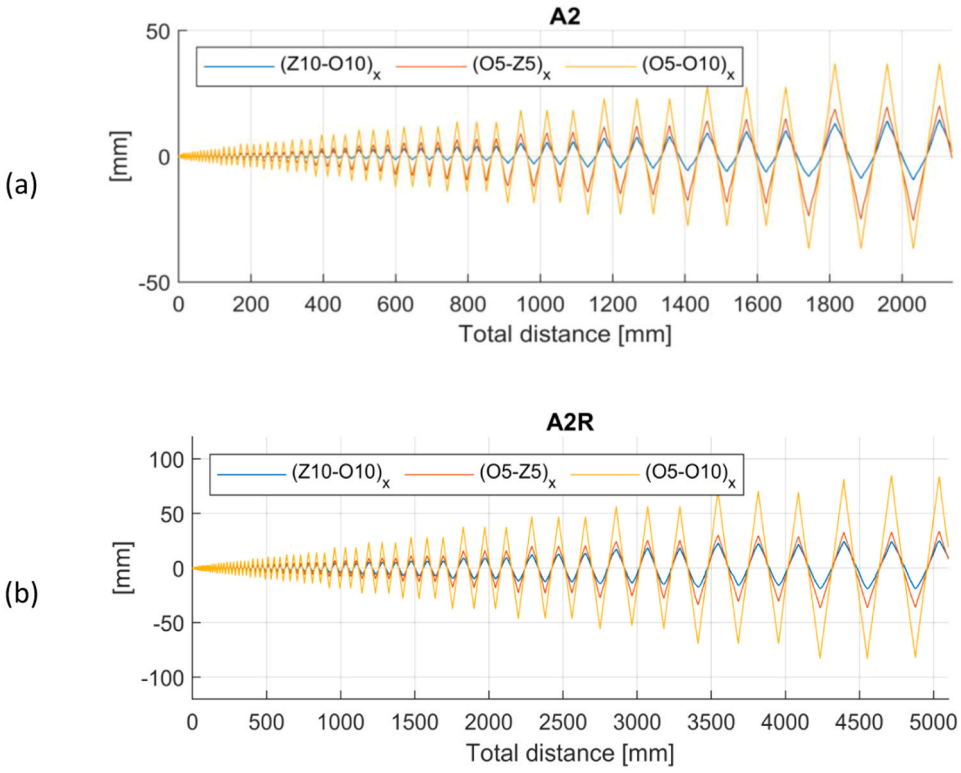

Fig. 7. Sliding at the top and at the bottom infill-RC beam interface and the imposed drifts to the specimen during the test: (a) A2 specimen; (b) A2R specimen; reference points are shown in Fig. 1, labels refer to the x-component of the relative displacement of two reference points.

at the bottom corner brick regions, the load drift curve in Fig. 8b indicates insignificant base shear load drop. Since the brick wall has the holes at the vertical direction, it accumulates minor damage for large frame horizontal drifts while it maintains most of its vertical load capacity. Moreover, the infill interaction significantly affected the global stiffness of the frame, but it started degrading at 0.25 % drift. In case of the strengthened specimen A2R, no stiffness degradation was observed throughout the test up to 3 % drift (see Fig. 8d).

Furthermore, the comparison of the shear strain on RC frame and in the infill during the cyclic shear tests of specimens A2 and A2R was computed. Shear strain was computed based on Aramis DIC measurements using diagonal deformation measurements of the RC frame and of the infill (see Fig. 9a). The results are shown in Figs. 9b and 9d for the initial loading phases of specimens A2 and A2R and in Fig. 9c for the entire test of specimen A2 separately. It was observed that in the initial loading cycles, the frame and the infill work more harmoniously and the behavior in both loading directions is fairly similar. In the next loading cycles, this coherence decreases as the frame and the infill strains are no longer identical. In the case of A2R it was noticed that in the further loading phases the strains of the RC frame are approximately equal in both loading directions, while the strains of the infill are time-aligned, but the equilibrium position has shifted slightly to the negative (left) loading direction. Probably the reason for such behavior is the damage that occurred in the infill and in the RC frame-infill interface during the test. This aspect is discussed later in the analysis of the CivEng Vision DIC results.

Important evidence on the efficiency of strengthening with FRPU is shown in Fig. 10, which shows the ratio of shear strains between the infill and the RC frame during the test for both specimens.

It can be seen that the ratio of shear strains for the A2 specimen is slightly higher at the beginning of the test, which means that a relatively larger portion of the load is carried by the infill, while this ratio decreases significantly by the end of the test. In contrast, in the case of the A2R specimen, the ratio of shear strains of the infill to the RC frame is slightly lower due to previous damage. For the next stages and until the end of the test, the ratio of shear strains between the infill and the RC frame remains at a relatively high level, which confirms the efficiency of the applied strengthening technique, as the in-plane and out-of-plane integrity of the infill is preserved. Additionally, the graph shows that the infill's ability to dissipate energy is improved due to its effective connection to the RC frame.

Maximum seismic resistance at the ultimate limit state (ULS) for the tested specimens as well as the dissipated (hysteretic) energy (calculated using the area of the hysteretic loops) up to drift of 1.60 % and up to the last phase of the individual test are presented in Table 2. Comparison of maximum resistance of tested specimens shows that infills increased maximum load capacity by 19 %, while the strengthening of the specimen A2 after loss of the infill-frame bond increased the maximum load capacity for additional 17 %, which is 36 % the capacity of RC frame without infill. The results of dissipated energy show that strengthening the A2 specimen increased the dissipated energy for more than 5 % at drift level of 1.60 %, while at the end of the test the strengthened specimen A2R dissipated 3.5-times the corresponding energy of the unstrengthened specimen A2 (being about to collapse in out-of-plane failure mode).

Additional information was provided by the CivEng Vision DIC system. Detailed measurements allowed to determine separate components of strains in horizontal X direction ε_X, in vertical Y direction ε_Y and shear strains $\varepsilon_{XY} = \gamma_{XY}/2$ as well as to compute principal tensile strains ε_1 and principal compression strains ε_2.

Maps of strains (ε_X, ε_Y, ε_{XY}, ε_1 – denoted as E1, ε_2 – denoted as E2), for the A2R specimen at drift level of 1.6 % are presented for the strain scale up to 0.01 [-] in Fig. 11. Values of principal stresses in the range of 0.6–0.9 % are randomly distributed over the whole FRPU strengthening surface, indicating that flexible PU matrix evenly distributes stress between all mesh fibers, except local areas in corners and top and bottom interfaces where detachment between infill and frame occurred. Tensile principal stress in Fig. 11d clearly shows that in the crushed corners on

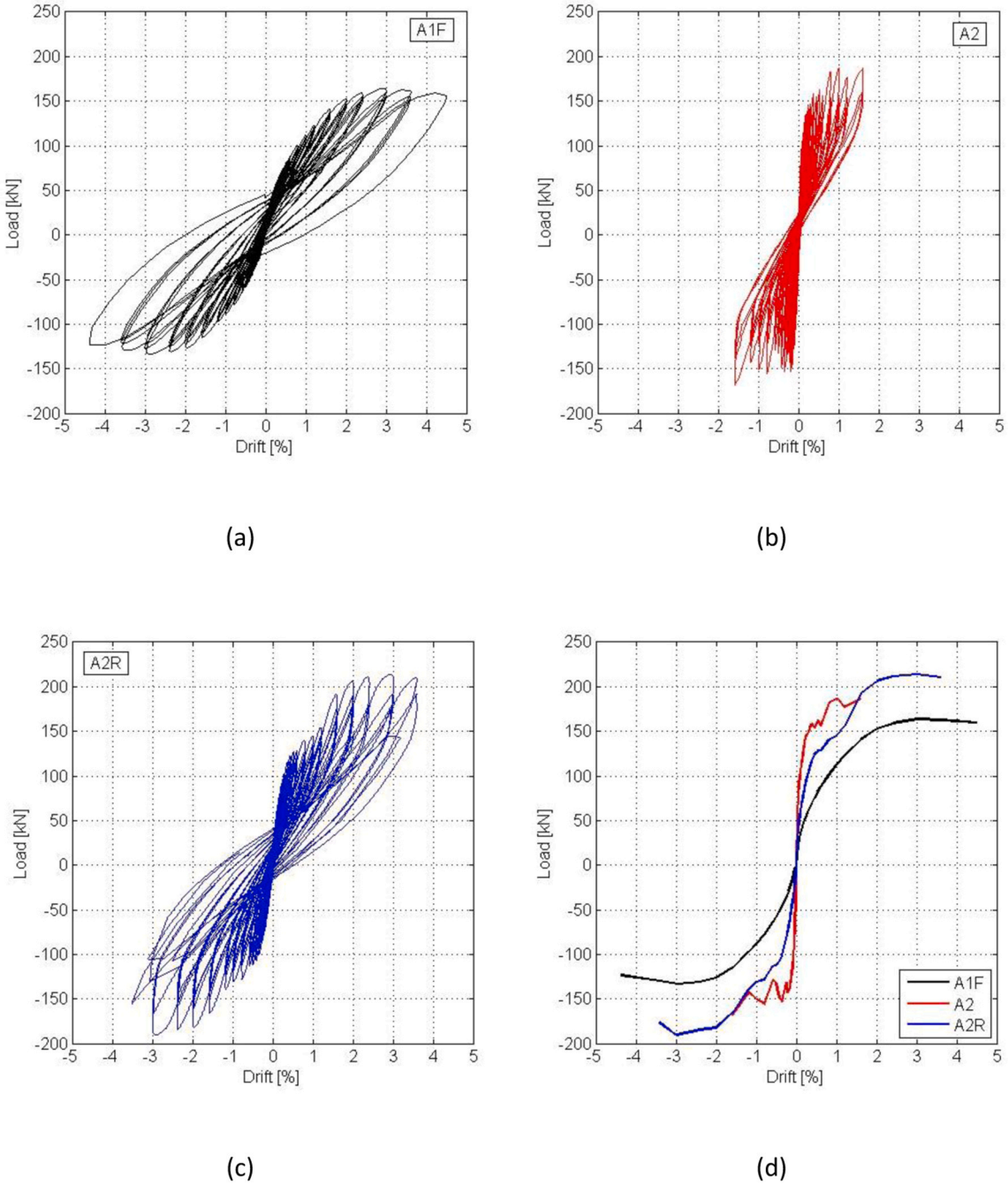

Fig. 8. Load-drift curves in the range + /- 4.3 % (up to displacement 110 mm): (a) specimen A1F; (b) specimen A2; (c) specimen A2R; (d) envelope curves of the specimens.

tensile strut only FRPU composite carries tensile stress (see also Fig. 13a) with dominant effort of the glass fiber net. Next, the fibers anchored in flexible PU matrix bonded to the masonry substrate, transfer partially tensile stress into shear stress redistributed over large area of the infill wall. The more or less uniform distribution of stress over the central part of the wall surface, due to the PU matrix flexibility, confirms also failure mode (Fig. 15b) where the inner part of the wall is totally crushed and the outer one is in good shape (protected by FRPU layer). Analysis of component strains ε_X, ε_Y, and ε_{XY} (Fig. 11a-c) indicates that participation of shear strain ($\varepsilon_{XY} = 0.9$ %) is dominant compared to other strains (ε_X, $\varepsilon_Y = 0.2$ %).

Similar presentation is shown in Fig. 12 for the drift level of 3.6 %. Strain maps for the ultimate drift of 3.6 % also confirm rather uniform strain distribution of principal stresses in the whole area of the FRPU strengthening. Even distribution of FRPU strengthening strains confirms that this kind of infill protection is resistant to cyclic loading, even if masonry elements are damaged under the mesh. Flexible PU matrix protects GFRP mesh fibers (vulnerable to stress concentration) against deteriorating influence of cracks and crushed sharp masonry particles by reduction of stress peaks and their even redistribution over mesh fibers.

This conclusion is also confirmed by the visible principal tensile strain levels in singular mesh fibers (Fig. 13a) presented for 1.6 % drift when serious damage process did not start and proper scale of CivEng Vision DIC analysis (up to 3 %) is adjusted. Focus on the strain distribution in the corner clearly indicates that locally occurred high strain level is smoothly propagated to larger area of the bonded FRPU strengthening, as it was shown in [29]. DIC analysis confirmed that FRPU strengthening is engaged in the whole volume of the composite

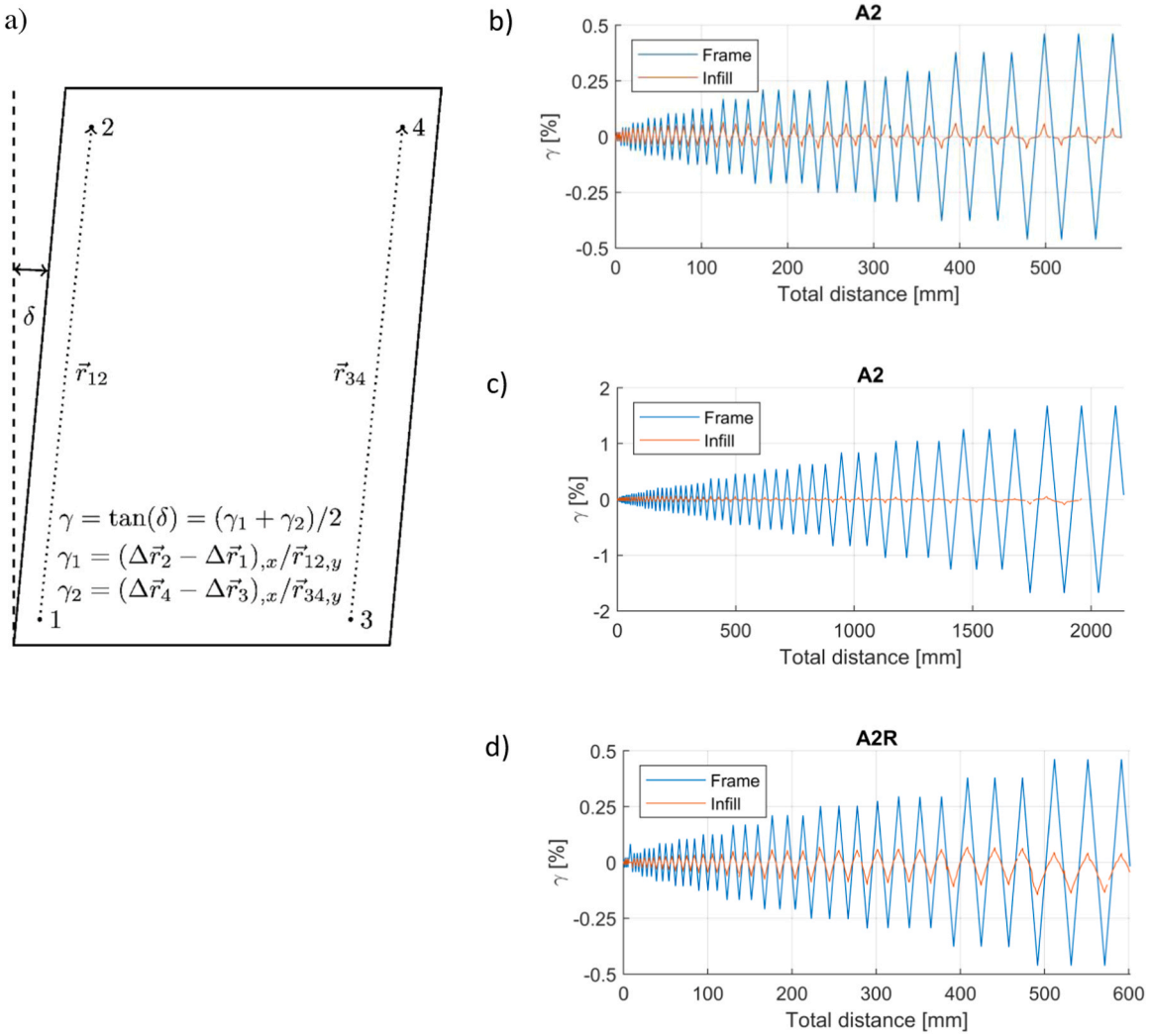

Fig. 9. Shear strain of the specimens: (a) definition of shear strain; (b) specimen A2 up to 0.44 % drift; (c) specimen A2 for the entire test; (d) specimen A2R up to 0.44 % drift.

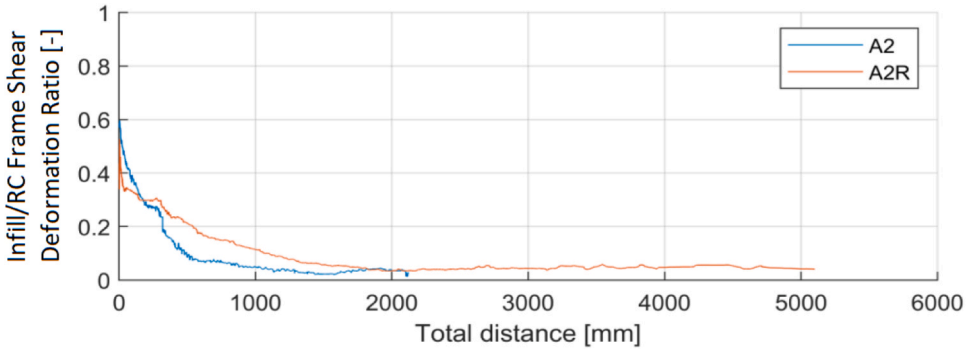

Fig. 10. Comparison of the ratio of the infill and RC frame shear deformation for specimens A2 and A2R.

covering the infill when tensile principal strains are activated during the frame deformation. Simultaneously, the FRPU strengthening does not constrain redistribution of compression principal strains E2 within the masonry infill (Figs. 11e and 12 e) in form of compression strut. However, information about real distribution of these strains under the flexible strengthening cover is difficult to be determined with the DIC analysis, because the observed FRPU deformations do not reflect directly hidden strain changes (also local cracks) in the masonry infill (see [29]). This is caused by changing of shear stiffness at the flexible interface masonry-to-composite. However, compression principal strains E2 manifested large deformations in cracked and crushed corners under the FRPU cover. Anyway, DIC was proved to reveal the unique behavior of FRPU, redistributing strain concentrations over larger area.

Another observation provided by the CivEng Vision DIC system allowed confirming information indicated by the Aramis DIC system regarding symmetrical/asymmetrical displacement of the infill versus

Table 2
Maximum Base Shear (F_{max}) and test termination for tested specimens (A1F, A2 and A2R) and dissipated (hysteretic) energy (E_{hys}) up drift of 1.6 % and up to the last phase of the test.

Specimen	At Maximum Base Shear		At Test Termination	E_{hys} [kNmm]	
	F_{max} (kN)	u (F_{max}) (mm)	u_{max} (mm)	1.6 % drift	At test termination
A1F	148.7 (100 %)	66.0	100.3	9.0×10^3 (38 %)	72.2×10^3 (300 %)
A2	177.5 (119 %)	29.3	36.2	24.0×10^3 (100 %)	24.0×10^3 (100 %)
A2R	202.3 (136 %)	66.1	81.2	25.3×10^3 (106 %)	83.6×10^3 (349 %)

the frame for small and large drifts. Analysis markers (No. 1–4), located at four infill-frame interfaces, are presented in Fig. 13b. They were used for determination of mutual slips changes (relative displacements) between the infill and the frame. Obtained results are presented in Fig. 14 for the A2R specimen.

Behavior of each analyzed point (Fig. 13b) of the interface is presented at the graphs with different colors, for the 3.6 % drift, taking for analysis almost one cycle of the frame movement. The extreme top, bottom, right and left slips are approximately equal: −5/+ 70 mm, −2/+ 41 mm, −2/+ 32 mm and −2/+ 32 mm, respectively. Such large differences are caused by a serious damage process in all infill corners under the FRPU strengthening (Fig. 6d) and uneven locking of the infill inside the frame, which is visible when movement to the left and to the right is compared. A severe damage in the top right corner accumulates deformation during moving the frame left, not allowing for developing the common compression strut in the infill that may cause infill collapse (Fig. 5d). On the other hand, and not seriously damaged, the top left corner causes pushing of the infill with generation of quite small principal compressive strains in this corner while moving on the right (Fig. 12e). All abovementioned measurements validate the strain redistribution potential of grids externally bonded with high deformability polyurethanes, engaging broader regions of the infill at lower stress intensities.

The applied FRPU system efficiently protected the detached infill against both out-of-plane and in-plane failure modes. In general, even sharp particles of crushed masonry blocks did not cause FRPU detachment or damage to glass fibers (Fig. 6d), because of stress redistribution introduced by the flexible polyurethane matrix. Finally, the A2R specimen was removed from the setup and the FRPU protected infill (A2R – already tested) was cut from the frame using a knife (Fig. 15). The infill with the crushed blocks inside was still consolidated (solid) and protected against moving out, even during out-of-plane movement forced horizontally by hand.

3.2. Thermal analysis

The presented FRPU emergency application, protecting an infill wall detached from a RC frame in the in-plane mode, can work in elevated

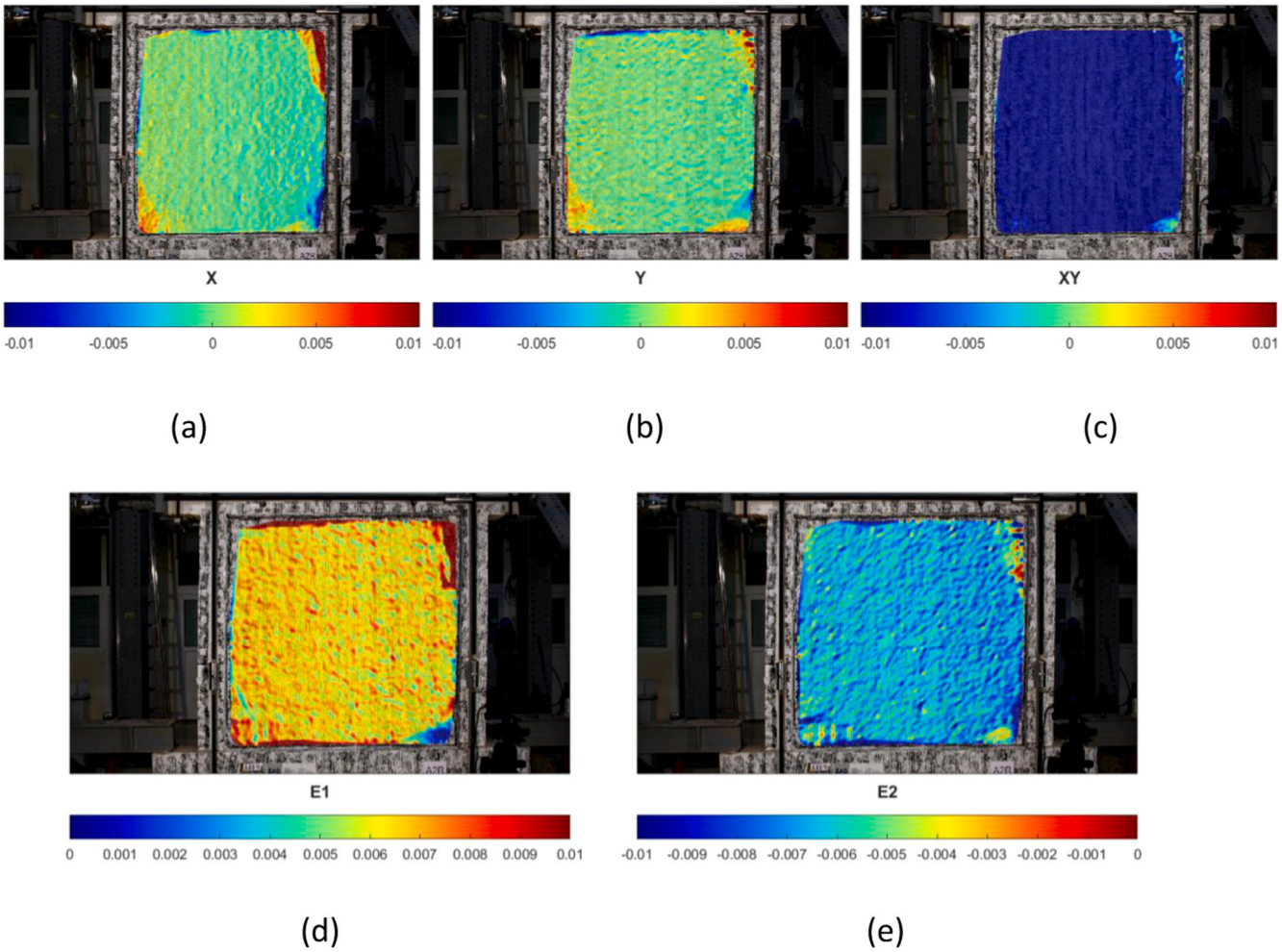

Fig. 11. CivEng Vision DIC strains maps for the A2R specimen at drift level of 1.6 % presented in the scale up to 0.01 [-]: (a) ε_X; (b) ε_Y; (c) ε_{XY}; (d) ε_1; (e) ε_2.

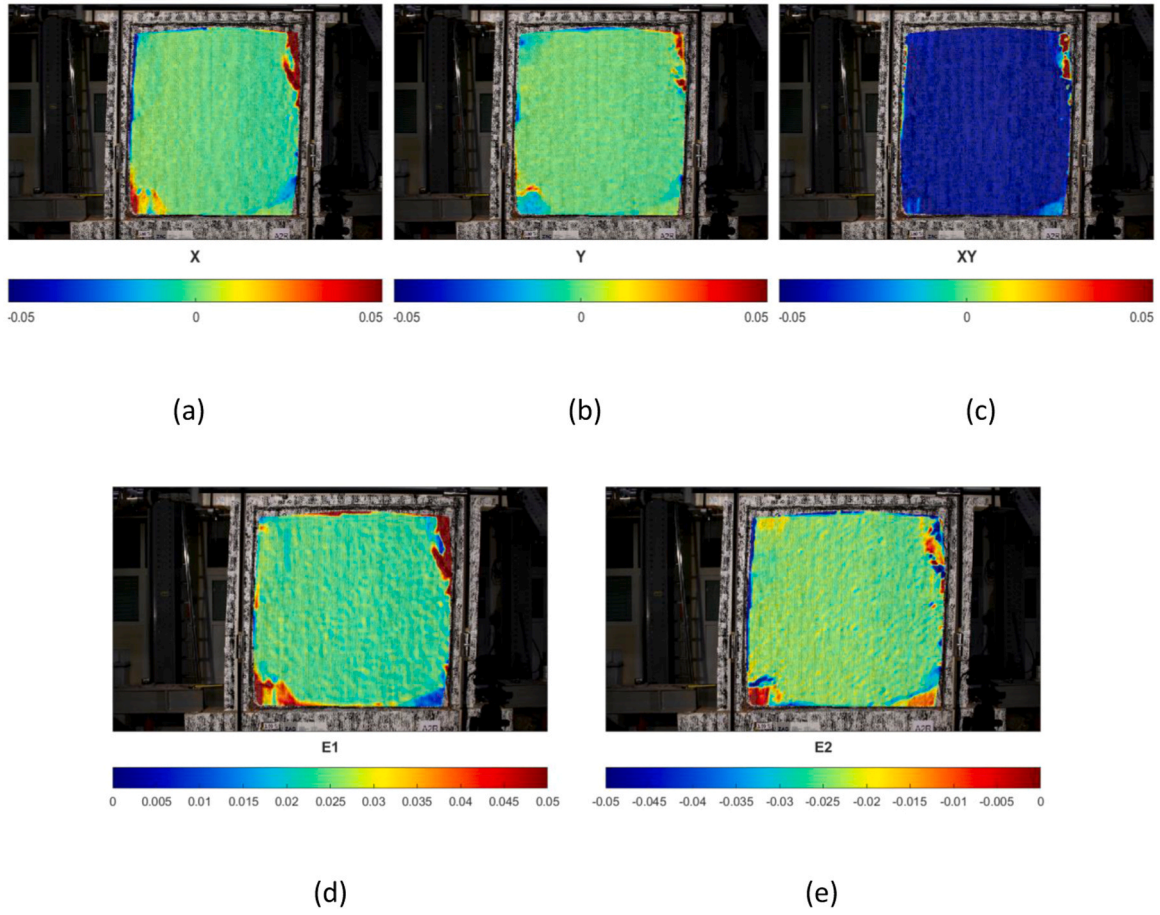

Fig. 12. CivEng Vision DIC strains maps for the A2R specimen at drift level of 3.6 % presented in the scale up to 0.05 [-]: (a) $\varepsilon_{X;}$ (b) ε_{Y}; (c) ε_{XY}; (d) ε_{1}; (e) ε_{2}.

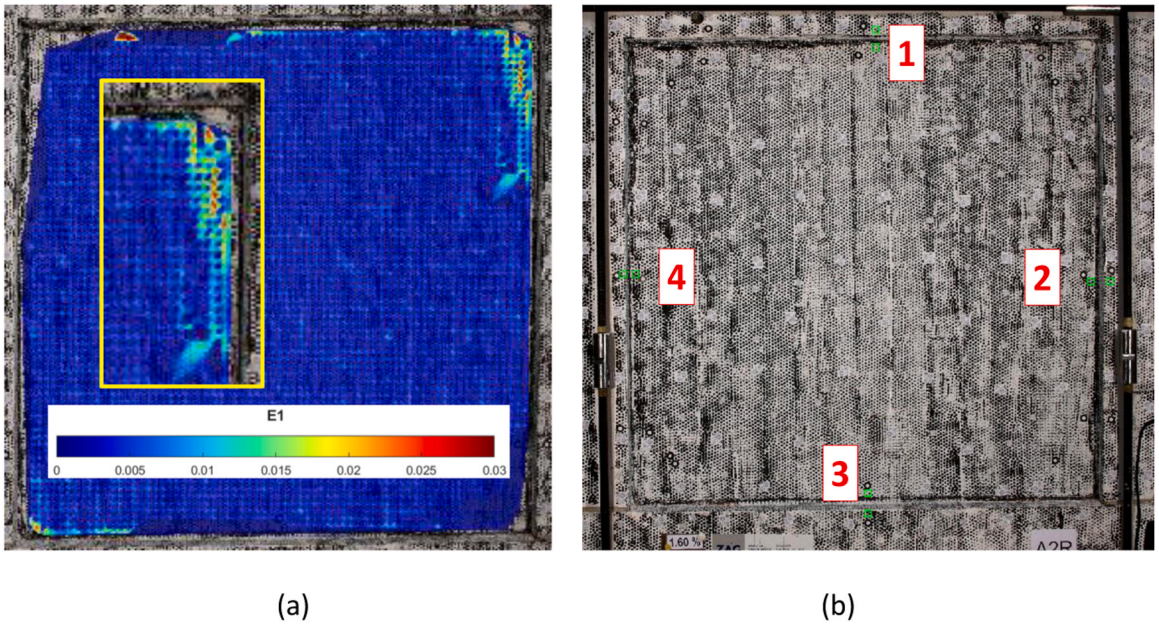

Fig. 13. (a) Strain redistribution in mesh for the A2R specimen at drift level of 1.6 %; (b) numeration of interface markers used for calculation of mutual slips between infill and frame.

temperatures present in civil engineering use in hot countries, thus FRPU must be resistant to them and its mechanical properties must be stable for the safe use. Evaluation of FRPU stability is required in this case, having in mind unstable properties of polymeric epoxy resins in elevated temperatures (over 60 °C). Dark color of the PU matrices using in FRPU additionally activates temperature increase in the composite.

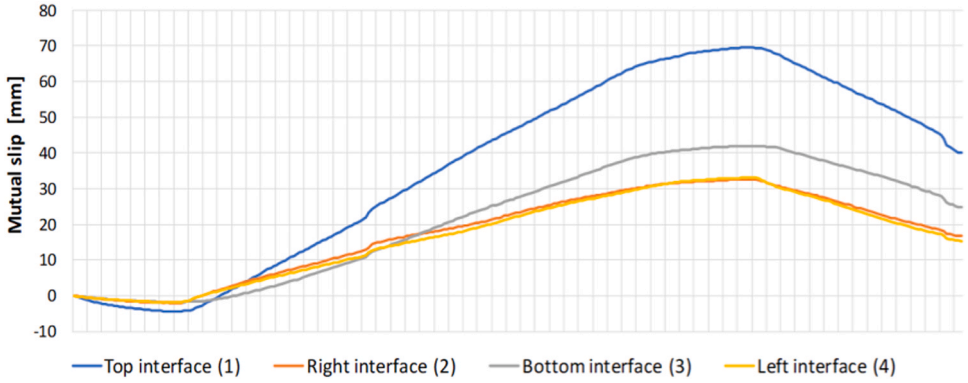

Fig. 14. Mutual slip change at the infill-frame interfaces of specimen A2R presented in one cycle for the drift level of 3.6 %.

Fig. 15. View of A2R specimen after removing from the setup: (a) part of FRPU after cutting (using knife); (b) demolished infill but still consolidated (solid) by FRPU protection - cut from the frame (using knife).

This forces the requirement of an elevated temperature determination for the PU matrices, which limits the stable PU mechanical properties and the safe use, as the infill-frame connection resistant to failure mechanism.

In terms of civil engineering, the obtained results of the thermal analysis should be examined in two different aspects. The first considers the temperatures that occur when the system is operating under normal conditions. The second aspect concerns the higher temperatures that may occur only during emergency cases e.g. fire caused in the aftermath of an earthquake. Under normal conditions, the most vulnerable part of the material is the one exposed to solar radiation. On a sunny day, the irradiated surface may reach a temperature twice as high as the air temperature. Table 3 shows the maximum temperature of the carbon fiber composite embedded in three different polyurethane matrixes and in one epoxy resin matrix, measured by a laser thermometer at the sun exposed surface (in the south of Poland, Cracow, June 28, 2020), collected when air temperature in shadow was reaching 30 °C. The control temperature 39.5 °C was measured on the white (sun exposed) plaster for a comparison. The temperature of the epoxy resin 61.2 °C was only a few degrees lower than in the case of polyurethane matrixes 65.5 – 67.7 °C, because of differences in color (PU – black, epoxy grey). However, the temperature of epoxy resin was above the limit of the thermal stability of the S330 epoxy material (45.0 °C), thus loss of the composite strength properties is expected due to overcoming of the glass transition temperature in the epoxy matrix. On the other hand, polyurethane matrix is assumed to be resistant to elevated temperatures up to 200 °C.

Table 3
The maximal temperatures reached on the surfaces of the different matrices in carbon fiber composites as the effect of solar radiation. The control temperature was measured on the white (sun exposed) plaster for a comparison, when air temperature in the shade was reaching 30 °C (June 28, 2020, Cracow, Poland).

Matrix material	Max. temperature [°C]	Control [°C]
Epoxy resin S330	61.2	39.5
PU PS	66.2	
PU PST	65.5	
PU PT	67.7	
PU	200	

Seismic protective technologies should be able to work at higher temperatures, since the seismic areas of the world are often in the regions of a hotter climate (e.g. California, the Caribbean, Turkey or Greece). The following results of the thermal analysis show that polyurethane adhesives meet these conditions.

In Fig. 16a, the results of the dilatometric analysis are shown with some close-ups of the most important parts and three HSM pictures showing the analyzed PU specimen at different temperatures (Fig. 16c-e). In the beginning, the polymer increased its dimensions gradually. Right above 140 ºC occurred some reorganization within the structure that led to slowing down the rate of elongation. The sample Kept its shape but smoothened its surface (Fig. 16d) which reduces the surface energy. This indicates some microscale effect, however, it has a very

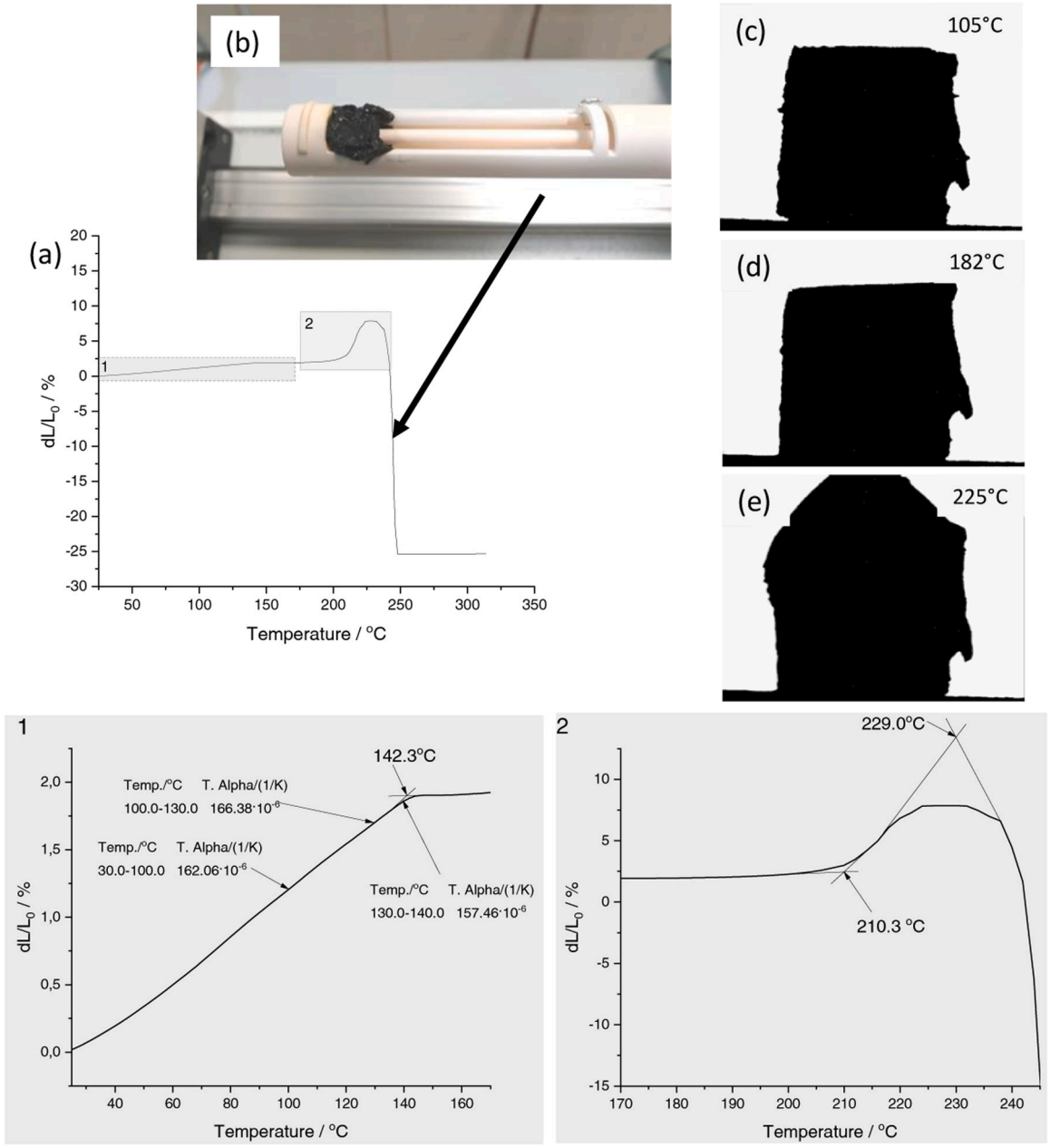

Fig. 16. (a) Dilatometric curve of the PS type polyurethane, (b) sample after maximum was reached, and HSM pictures of the sample heated to (c) 105 °C, (d) 182 °C, and (e) 225 °C.

minor influence on the performance of the material in terms of its mechanical properties. Up to 200 ºC, no other effect was observed. Then, the material starts expanding rapidly (Fig. 16e).

The dilatometric curve reached the maximum at 229 ºC before the sudden decrease. The specimen continued to grow, but began to behave like a delicate foam as a result of the first stage of degradation. The sample was no longer able to withstand the pressure of the apparatus needle (0.01 N) penetrating the material, making it impossible to continue the measurement. The photo in Fig. 16b shows the PU sample right after the maximum was reached. The specimen's failure occurred above 200 ºC which is supposed to be far enough from the range of temperatures that occur in everyday conditions in hot countries.

The TGA and DSC analyses for PU are presented with the HSM pictures corresponding to the observed effects at the higher temperatures in Fig. 17. The DSC curve shows no thermal effect up to 204 ºC. This confirms that the effect observed in the dilatometric study at 140 ºC did not cause any damage to the material. The initial mass loss of 1.07 % is the result of damping of water and other volatile compounds. After the first thermal effect, when the rapid expansion occurred, a mass loss of 4.29 % was observed. The following stages of degradation are expressed by two more thermal effects at 294 ºC and 406 ºC and led to a total mass change of 43.12 %.

Although the mass loss is very notable, it did not cause any further changes in the morphology of the specimen (Fig. 17c, d). The last effect at 479 ºC was followed by a slight change of the sample's shape, resembling subsidence, probably due to advanced degradation. The further heating led to the gradual collapsing of the sample.

Despite the oxygen-rich conditions, self-ignition of PU was not observed. In the case of fire, the material would work mechanically until the first thermal effect detected by the DSC. Then, the outer layer would rapidly expand to the foam-like structure, isolating the inner layers of the composite and slowing down the heating process. This would allow

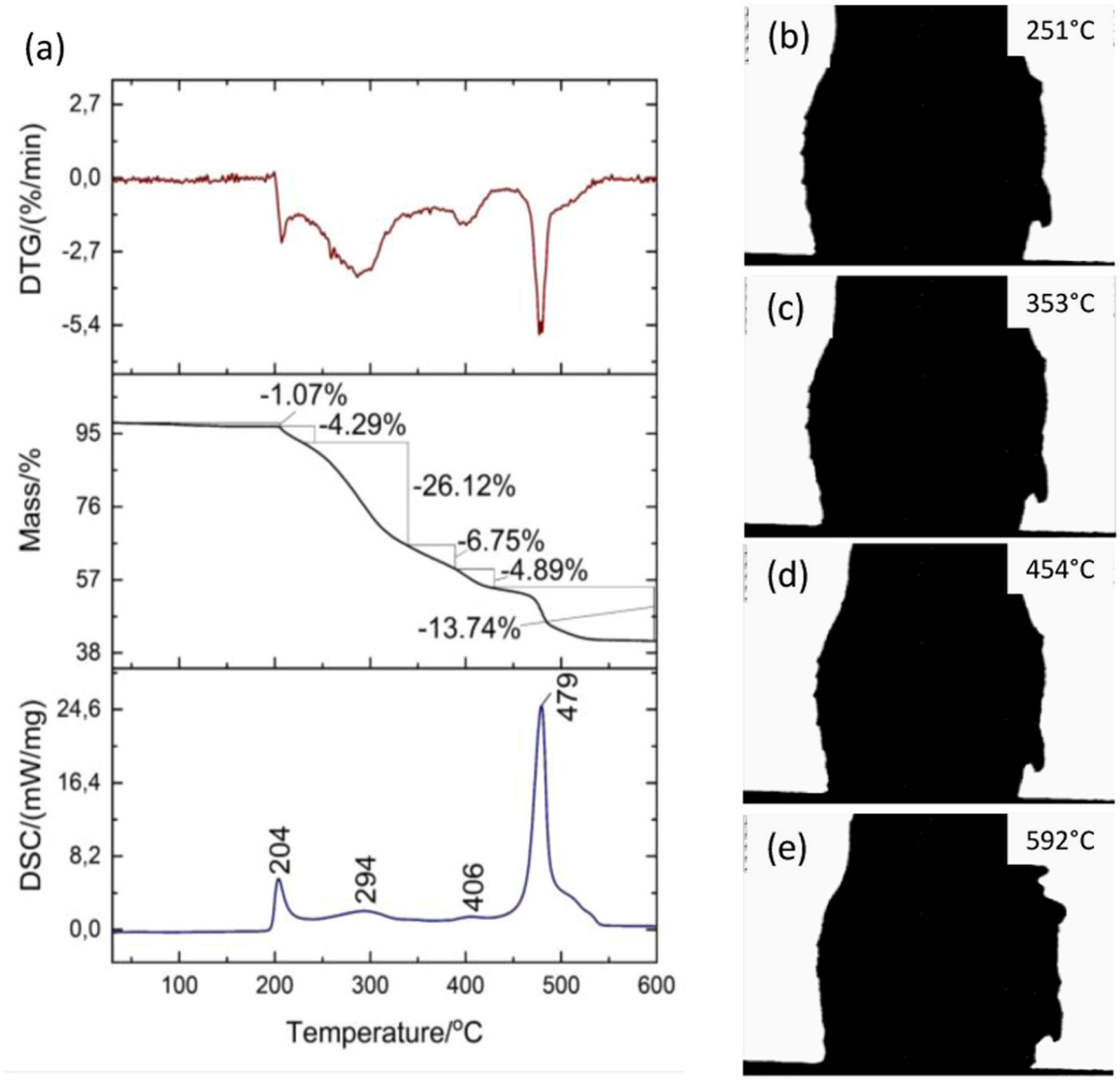

Fig. 17. (a) TGA-DSC curves of the PS type polyurethane, and HSM pictures showing the sample after each detected thermal effect at (b) 251 °C, (c) 353 °C, (d) 454 °C, and (e) 592 °C.

the PU system to operate for longer time periods, before potential failure due to prolonged exposure to high temperatures. The material would probably perform in this manner until the last thermal effect detected by the DSC occurred (i.e. in 479 °C). The gradual collapse of the specimen's shape is the consequence of advanced chemical bond disintegration and over 40 % mass loss. At this stage of degradation, the material would probably slowly detach from the composite and simply fall off, no longer being useful.

4. Conclusions

In this study, in-plane seismic performance of RC frame without infill, RC frame with infill and RC frame with infill strengthened with FRPU under in-plane quasi static cyclic loads is presented. In addition, thermal tests of FRPU are included.

The reference RC frame without infill was tested up to 4.30 % drift, at which level the seismic resistance of the specimen decreased in both loading directions. The damage occurred at the bottom of both RC columns. In the case of specimen A2, detachment at the frame-infill interface was observed at 0.44 % drift, while the complete detachment and crushing of the infill at the corners was evident at 1.60 % drift. At that stage, the cyclic shear test was stopped and the A2 specimen was strengthened using the FRPU system, which was applied on both sides of the specimen. After strengthening, the reinforced A2R specimen was retested under cyclic shear up to a drift of 3.60 %. During the test some rocking as well as some bulges in the infill corners behind the working FRPU strengthening were observed. At the ultimate stage no global FRPU detachment has been observed. At 1.60 % drift, the lateral resistance of the plain frame (A1F) increased by 39 % when the specimen had infills and at that loading stage it remained the same when retested in strengthened state. At the end of the tests, the absolute maximum resistance of the RC frame increased by 19 % when infill was present, while it increased by 36 % when the specimen had infills and FRPU strengthening. The application of FRPU also increased the ultimate drift from 1.60 % to 3.60 % and the energy dissipation by a factor of 3.5. The results presented in this study suggest that the FRPU strengthening of orthoblock brick infills may ensure ductile, stable and symmetric P-d behavior of the RC frames with increased bearing shear forces.

The DIC results, provided by the Aramis and the CivEng Vision system in synergy, allowed for visualization of strains' maps covering practically the whole area of the tested specimens and for computing locally required information about behavior of highly deformable interfaces. Classical measurement methods (e.g. using LVDTs) provide information limited to tone point and one direction but in constrained

range. Properly scaled DIC strain maps, showed the location of damage initiation on specimen surfaces, uncovered and covered by the FRPU strengthening system. Moreover, they could quantify distribution of strains over the entire measuring surface, indicating the location of damage, even prior to their visual appearance. The obtained results confirmed the assumption that the flexible matrix of the FRPU strengthening system reduces stress concentration peaks and re-distributes them more evenly over the entire composite surface. High flexibility of the polyurethane matrix assures high bond strength to the masonry and concrete substrates by this redistribution and gradually transfer shear strains to the mesh fibers, protecting them against high stresses generated by cracks appearing in masonry infills and sharp particles in places of crushing. Mutual slips at interfaces and composite strain efforts, determined by DIC analysis for various types of strains, confirmed high efficiency of the FRPU strengthening system, able to withstand very high local deformations occurring cyclically. However, DIC results are related only to the visible surface and cannot be simply extended to the infill behavior hidden beneath the flexible polyurethane matrix.

The solar heating measurement confirmed that the temperatures of the regular conditions might be in some cases too high to use epoxy resins safely. Polyurethane adhesives may be the solution to this problem, as they retain their mechanical properties up to around 200 °C. Above this temperature, degradation and loss of mechanical properties occur, however the material expands rapidly to a foam-like structure that may form a barrier to protect the inner layers of the composites from heating in the case of fire. The outer layer would probably protect the rest of the system until it reaches around 500 °C. At this temperature, the material is so degraded that it slowly loses its integrity. This conclusion however requires confirmation based on more detailed fire tests.

CRediT authorship contribution statement

Alberto Viskovic: Validation, Conceptualization. **Petra Triller:** Writing – review & editing, Writing – original draft, Visualization, Validation, Supervision, Resources, Project administration, Methodology, Investigation, Funding acquisition, Conceptualization. **Konrad Kwiecień:** Writing – review & editing, Writing – original draft, Visualization, Software, Resources, Investigation, Formal analysis, Data curation. **Arkadiusz Kwiecień:** Writing – review & editing, Writing – original draft, Visualization, Validation, Supervision, Resources, Project administration, Methodology, Investigation, Funding acquisition, Formal analysis, Data curation, Conceptualization. **Magdalena Szumera:** Writing – review & editing, Writing – original draft, Visualization, Software, Resources, Investigation, Formal analysis, Data curation. **Theodoros Rousakis:** Writing – review & editing, Writing – original draft, Validation, Supervision, Project administration, Methodology, Investigation, Funding acquisition, Conceptualization. **Vachan Vanian:** Writing – review & editing, Writing – original draft, Resources, Formal analysis, Conceptualization. **Ahmet Tugrul Akyildiz:** Writing – original draft, Resources, Investigation, Formal analysis, Conceptualization. **Uroš Bohinc:** Visualization, Software, Resources. **Bogusław Zając:** Resources, Investigation, Conceptualization. **Marcin Tekieli:** Visualization, Software, Resources, Investigation, Data curation.

Declaration of Competing Interest

The authors declare that they have no known competing financial interests or personal relationships that could have appeared to influence the work reported in this paper.

Data availability

Data will be made available on request.

Acknowledgements

This research activity was within the framework of the Research Project: “In- and out-of-plane tests of masonry-infilled RC frames with flexible joints” - Cooperation Agreement between ZAG - Slovenian National Building and Civil Engineering Institute (Ljubljana, Slovenia), Cracow University of Technology (Cracow, Poland) and Democritus University of Thrace (Xanthi, Greece). Authors acknowledge the materials support provided by Sika Poland company and KEBE Northern Greece Ceramics. Thermal studies were performed within the framework of funding for statutory activities of AGH University of Science and Technology in Krakow, Faculty of Materials Science and Ceramics (16.16.160.557).

References

[1] EERI. Northridge earthquake (January 17, 1994) preliminary reconnaissance report. Oakland, CA: 1994.
[2] Decanini LD, De Sortis A, Goretti A, Liberatore L, Mollaioli F, Bazzurro P. Performance of reinforced concrete buildings during the 2002 Molise, Italy, Earthquake. Earthq Spectra 2004;20:221–55. https://doi.org/10.1193/1.1765107.
[3] Li B., Wang Z., Mosalam K.M., and Xie H., “Wenchuan Earthquake Field Reconnaissance on Reinforced Concrete Framed Buildings with and without Masonry Infill Walls” *14th World Conference on Earthquake Engineering, 12–17 October 2008, Beijing, China.*
[4] Murty C.V.R. and Jain S.K., “Beneficial influence of masonry infill walls on seismic performance of RC frame buildings” *12th World Conference on Earthquake Engineering, 30 January–4 February 2000, Auckland, New Zealand.*
[5] Asteris PG. Lateral stiffness of brick masonry infilled plane frames. J Struct Eng 2003;vol. 129(8):1071–9. https://doi.org/10.1061/(ASCE)0733-9445(2003)129:8(1071).
[6] Viskovic A, Zuccarino L, Kwiecień A, Zając B, Gams M. Quick seismic protection of weak masonry infilling in filled framed structures using flexible joints. Key Eng Mater 2017;vol. 747:628–37.
[7] Ricci P, Di Domenico M, Verderame GM. Empirical-based out-of-plane URM infill wall model accounting for the interaction with in-plane demand. Earthq Eng Struct Dyn 2018;vol. 47(3):802–27. https://doi.org/10.1002/eqe.2992.
[8] Pasca M, Liberatore L. Predicting models for the evaluation of out-of-plane ultimate load carrying capacity of masonry infill walls. Earthquake Resistant Engineering Structures *X*,WIT Transactions on The Built Environment, Vol 152. WIT Press,; 2015. https://doi.org/10.2495/ERES150071.
[9] Pujol S, Fick D. The test of a full-scale three-story RC structure with masonry infill walls. Eng Struct 2016;Vol. 15:48–63. https://doi.org/10.1016/j.engstruct.2015.12.013.
[10] Kallioras S., Pohoryles D.A., Bournas D., Molina F.J., Pegon P., “Seismic performance of a full-scale five-story masonry-infilled RC building subjected to substructured pseudodynamic tests”, Earthquake Engineering & Structural Dynamics, Vol. 52, Issue 12, pp. 3649–3678, doi.org/10.1002/eqe.3940.
[11] Dafnis A, Kolsch H, Reimerdes H-G. Arching in masonry walls subjected to earthquake motions. J Struct Eng 2002;128:153–9. https://doi.org/10.1061/(ASCE)0733-9445(2002)128:2(153).
[12] Preti M, Migliorati L, Giuriani E. Experimental testing of engineered masonry infill walls for post-earthquake structural damage control. Bull Earthq Eng 2015;vol. 13(7):2029–49. https://doi.org/10.1007/s10518-014-9701-2.
[13] Vailati M, Monti G. Earthquake-resistant and thermo-insulating infill panel with recycled-plastic joints. In: D’Amico S, editor. Earthquakes and Their Impact on Society. in Springer Natural Hazards, Cham: Springer International Publishing; 2016. p. 417–32. https://doi.org/10.1007/978-3-319-21753-6_15.
[14] Muthu Kumar S, Satyanarayanan KS. Study the effect of elastic materials as interface medium used in infilled frames. Part 3 Mater Today Proc 2018;vol. 5(2):8986–95. https://doi.org/10.1016/j.matpr.2017.12.343.
[15] Günaydin, et al. Seismic damage assessment of masonry buildings in Elazığ and Malatya following the 2020 Elazığ-Sivrice earthquake, Turkey. Bull Earthq Eng 2021;vol. 19(6):2421–56. https://doi.org/10.1007/s10518-021-01073-5.
[16] Angın Z. Lessons learned from the past earthquakes on building performance in Turkey. J Struct Eng Appl Mech 2020;vol. 3(2):61–84. https://doi.org/10.31462/jseam.2020.02061084.
[17] De Martino G, Di Ludovico M, Prota A, Moroni C, Manfredi G, Dolce M. Estimation of repair costs for RC and masonry residential buildings based on damage data collected by post-earthquake visual inspection. Bull Earthq Eng 2017;vol. 15(4):1681–706. https://doi.org/10.1007/s10518-016-0039-9.
[18] Erdem I, Akyuz U, Ersoy U, Ozcebe G. An experimental study on two different strengthening techniques for RC frames. Eng Struct 2006;vol. 28(13):1843–51. https://doi.org/10.1016/j.engstruct.2006.03.010.
[19] Yuksel E, et al. Performance of alternative CFRP retrofitting schemes used in infilled RC frames. Constr Build Mater 2010;vol. 24(4):596–609. https://doi.org/10.1016/j.conbuildmat.2009.09.005.
[20] Preti M., Bolis V., and Stavridis A., “Design of masonry infill walls with sliding joints for earthquake structural damage control,” in *Proceedings of the 16th International Brick and Block Masonry Conference, 26–30 June 2016, Padova, Italy* pp. 1317–1324. doi: 10.1201/b21889–163.

[21] Facconi L, Minelli F, Giuriani E. Response of infilled RC frames retrofitted with a cementitious fiber-mesh reinforced coating in moderate seismicity areas. Constr Build Mater 2018;vol. 160:574–87. https://doi.org/10.1016/j.conbuildmat.2017.11.033.
[22] Ismail N, El-Maaddawy T, Khattak N. Quasi-static in-plane testing of FRCM strengthened non-ductile reinforced concrete frames with masonry infills. Constr Build Mater 2018;vol. 186:1286–98. https://doi.org/10.1016/j.conbuildmat.2018.07.230.
[23] De Sousa C, Barros JAO, Correia JR. In-plane cyclic behaviour of RC frames strengthened with composite sandwich panels. Eng Struct 2022;vol. 251:113529. https://doi.org/10.1016/j.engstruct.2021.113529.
[24] Arslan ME, Aykanat B, Ayyıldız MA, Subaşı S, Maraşlı M. Effects of basalt and glass fiber composites usage for strengthening on the cyclic behavior of brick infill walls. J Build Eng 2022;vol. 52:104405. https://doi.org/10.1016/j.jobe.2022.104405.
[25] Zima K., Wieczorek D., Kwiecień A. "Analysis of selected aspects of the life cycle for flexible joints between reinforced concrete frames and masonry infills". In *Proceedings of International Conference on Istanbul and Earthquake 2022 (ICE'2022)*, Istanbul Aydin University Publications, pp. 11–29, 2022, ISBN: 978 625 7783 48 4.
[26] Gams M, Kwiecień A, Zając B, Tomaževic M. "Seismic strengthening of brick masonry walls with flexible polymer coating. In: Lourenço PB, Haseltine B, Vasconcelos G, editors. In Proc., 9th International Masonry Conf., 7-9 July. *Guimarães, Portugal*: International Masonry Society; 2014.
[27] Triller P, TomaževičM, Lutman M, Gams M. "Seismic Behavior of Strengthened URM Masonry – An Overview of Research at ZAG,". Procedia Eng Jan. 2017;vol. 193:66–73. https://doi.org/10.1016/j.proeng.2017.06.187.
[28] Bolhassani M, Rajaram S, Hamid AA, Kontsos A, Bartoli I. "Damage detection of concrete masonry structures by enhancing deformation measurement using DIC," in Nondestructive Characterization and Monitoring of Advanced Materials. Aerospace, and Civil Infrastructure 2016. SPIE,; 2016. p. 227–40. https://doi.org/10.1117/12.2218368.
[29] Tekieli M, De Santis S, de Felice G, Kwiecień A, Roscini F. Application of digital image correlation to composite reinforcements testing. Compos Struct 2017;vol. 160:670–88. https://doi.org/10.1016/j.compstruct.2016.10.096.
[30] Koutas L, Bousias SN, Triantafillou TC. Seismic strengthening of masonry-infilled RC Frames with TRM: Experimental Study. J Compos Constr 2015;Vol. 19(No. 2). https://doi.org/10.1061/(ASCE)CC.1943-5614.0000507.
[31] da Porto F, Guidi G, Verlato n, Modena C. Effectiveness of plasters and textile reinforced mortars for strengthening clay masonry infill walls subjected to combined in-plane/out-of-plane actions. Mauerwerk 2015;Volume 19(Issue 5): 334–54. https://doi.org/10.1002/dama.201500673.
[32] Koutas L, Bournas DA. Out-of-plane strengthening of masonry-infilled RC frames with textile-reinforced mortar jackets. J Compos Constr 2018;Vol. 23(No. 1). https://doi.org/10.1061/(ASCE)CC.1943-5614.00009.
[33] Akhoundi F, Vasconcelos G, Lourenço P, Silva LM, Cunhac F, Fangueiro R. In-Plane Behavior of cavity masonry infills and strengthening with textile reinforced mortar. Eng. Struct. 2018;Vol. 156:145–60. https://doi.org/10.1016/j.engstruct.2017.11.002.
[34] García L.E., Varona B., Baeza F.J., Torres B., "Textile Reinforced Mortars (TRM) tensile behavior after high temperature exposure", Construction and Building Materials 328(1):127116, doi:10.1016/j.conbuildmat.2022.127116.
[35] Kapsalis P, Tysmans T, van Hemelrijck D, Triantafillou T. State-of-the-art review on experimental investigations of textile-reinforced concrete exposed to high temperatures. J Compos Sci 2021;5(11):290. https://doi.org/10.3390/jcs5110290.
[36] Koutas LN, Tetta Z, Bournas DA, Triantafillou TC. Strengthening of concrete structures with tex-tile reinforced mortars: state-of-the-art review. J Compos Constr 2019;23:03118001. https://doi.org/10.1061/(ASCE)CC.1943-5614.0000882.
[37] Raoof SM, Bournas DA. TRM versus FRP in flexural strengthening of RC beams: Behaviour at high temperatures. Constr Build Mater 2017;154:424–37. https://doi.org/10.1016/j.conbuildmat.2017.07.195.
[38] Tetta ZC, Bournas DA. TRM vs FRP jacketing in shear strengthening of concrete members sub-jected to high temperatures. Compos Part B: Eng 2016;106:190–205. https://doi.org/10.1016/j.compositesb.2016.09.026.
[39] Raoof SM, Bournas DA. Bond between TRM versus FRP composites and concrete at high temper-atures. Compos Part B: Eng 2017;127:150–65. https://doi.org/10.1016/j.compositesb.2017.05.064.
[40] Xie F, Zhang T, Bryant P, Kurusingal V, Colwell JM, Laycock B. Degradation and stabilization of polyurethane elastomers. Prog Polym Sci 2019;90:211–68. https://doi.org/10.1016/j.progpolymsci.2018.12.003.
[41] Kwiecień K, Kwiecień A, Stryszewska T, Szumera M, Dudek M. Durability of PS-polyurethane dedicated for composite strengthening applications in masonry and concrete structures. Art. no. 12 Polymers 2020;vol. 12(12). https://doi.org/10.3390/polym12122830.